Hydrodynamics of Droplet Generation Under Squeezing Regime in a T-junction Cylindrical Microfluidic System

Pratibha Dogra and Ram Prakash Bharti

1 Introduction

The interest in the study of fluid–fluid interaction in the microfluidic systems has escalated over the years because of its prodigious potential to accentuate the processes coupled with medical and industrial relevance [1]. The two-phase microfluidic systems are the most rudimentary and crucial domains in multiphase flows. The research in this area involves various aspects like droplet generation [2], movement [3], coalescence [4], etc. The manipulation and production of micron sized droplets involves employment of different geometric configurations and combinations, intrinsic properties of phases involved and external forces like magnetic and electrical fields. The generation and manipulation of these micron sized droplets is complex in terms of the production controllability, hence profound understanding of the droplet behavior is crucial, especially the breakup behavior. Apart from various geometric configurations available like co-flow, flow focusing devices [5, 6], the symmetric T-junction is an elementary domain for investigation of droplet breakup in microfluidics because of its ability to produce monodisperse droplets and simple geometry [7–9]. Use of microfluidic geometry to elucidate the instability leading to formation of the droplets was first done by [9] using T-shaped geometry with water/oil as dispersed and continuous phases. They saw various dynamic patterns evolving because of the geometry and interaction of both phases. The authors suggested that the droplet formation is dominated by the balance between the capillary force and the tangential shear force. A detailed experimental study of the T-junction configuration [7] identified the droplet formation under squeezing regime and predicted that the mechanism is directly related to the geometrical confinement in which droplet is forming. De Menech et al. [10] elucidated three distinct regimes for formation

P. Dogra · R. P. Bharti (✉)
Complex Fluid Dynamics and Microfluidics (CFDM) Lab, Department of Chemical Engineering, Indian Institute of Technology Roorkee, Roorkee, Uttarakhand 247667, India
e-mail: rpbharti@ch.iitr.ac.in

K. M. Singh et al. (eds.), *Fluid Mechanics and Fluid Power, Volume 5*, Lecture Notes in Mechanical Engineering, https://doi.org/10.1007/978-981-99-6074-3_6

of droplets in T-junction configuration, i.e., squeezing, dripping and jetting and concluded that droplet breakup in the squeezing regime is the result of pressure rise in the upstream. Christopher et al. [9] performed the experiments for the fluids with a higher viscosity in a T-junction microchannel. They reported that the droplet size and generation frequency (f) have a power relation with Capillary number (Ca). The effect of wetting properties on droplet shapes was studied by [11]. They predicted that the wetting behavior affects the pressure balance during the droplet formation. Both experimental and numerical effects of channel wettability on the droplet length was done by Bashir et al. [12]. They elucidated the strong impact of the contact angle on the droplet generation and pinch-off time. Kovalev et al. [13] have experimentally observed the 3D flow structures in droplet generation in rectangular cross section T-junction at low viscosity ratios (10^{-3}) of two phases. Boruah et al. [14] studied the effect of surface wettability on droplet dynamics. They did numerical investigation on the displacement behavior of a dispersed liquid column flowing through a microfluidic T-junction. They reported that surface wettability is a dominant factor in determining the interface evolution. Li et al. [10] numerically studied the impact of ribs on the droplet dynamics. They performed studies on the T-junction with varying size of ribs and found that incorporating ribs in T-junction offers good control over droplet formation. Later, they performed experiments on the same geometry and gave the scaling laws for the slug and the droplet length. Kalantarifard et al. [15] have explored the theoretical and experimental limits of monodispersed droplet generation. They explored underlying reasons for variation in droplet size. The dependence of bubble shape and size on the inertial force of the dispersed phase was presented by [16]. They gave scaling law for droplet size in terms of the dispersed phase inertial force. Study on interface evolution and droplet pinch-off was done by [17]. The authors explored the different pinch-off mechanisms under the squeezing regime at wide range of flow rate ratio ($0.1 < Q_r < 10$). In most of the studies, it has been predicted that the inertial force effects are negligible when talking about the droplet generation under the squeezing regime. There are many scaling laws available predicting the droplet size, but these are not universal, and hence the study of droplet generation under squeezing regime under different parameters becomes important in order to develop the correlations that can be universally applied. This work presents the effects of the inertial force at different contact angle and channel dimensions on the droplet generation.

2 Mathematical Modeling

2.1 Problem Statement

The problem involves the two-phase flow of Newtonian immiscible fluids under laminar, isothermal conditions through a T-junction cross-flow microfluidic system, as shown in Fig. 1. The diameter of both the main channel, carrying continuous phase

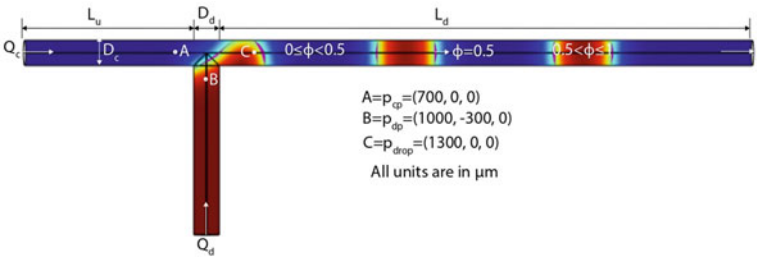

Fig. 1 Representation of the cylindrical T-junction microfluidic system

and the side channel, carrying dispersed phase is taken same ($D_d = D_c = 140$ μm and 280 μm). The length of main channel is $L = (L_u + D_d + L_d) = 5280$ μm and of side channel is $L_s = 1000$ μm. The continuous and dispersed phases flow through their respective channels at flow rates equal to Q_c μl/s and Q_d μl/s. At the channel outlet, static pressure condition is employed, and at the channel boundaries, no-slip condition is imposed. The mass transfer and phase change effects along the interface are ignored, also the contact angle is static and the surface tension acting at the fluid interface is assumed to be constant.

2.2 Governing Equations

The simplified continuity and momentum equations that governs the underlying physics involving multiphase flow are as follows:

$$\nabla \cdot \vec{V} = 0 \tag{1}$$

$$\rho(\Phi)\left[\frac{\partial \vec{V}}{\partial t} + \vec{V} \cdot \nabla \vec{V}\right] = -\nabla p + \nabla \cdot \tau + F_\sigma \tag{2}$$

where $\vec{V}$ and p are the velocity vector and pressure fields, respectively, and $\boldsymbol{\tau}$ is the deviatoric stress tensor.

$$\tau = 2\mu(\Phi)\vec{\boldsymbol{D}} \tag{3}$$

where $\vec{D}$ the rate of deformation tensor is defined as follows.

$$\vec{D} = \frac{1}{2}\left[(\nabla \vec{V}) + (\nabla \vec{V})^T\right] \tag{4}$$

For elucidating the topological changes at the interface separating the both fluids, conservative level set method is employed which is given by Eq. (5).

$$\frac{d\phi}{dt} + \vec{V}.\nabla\phi = \gamma\nabla.\phi' \tag{5}$$

$$\phi' = [\epsilon_{ls}\ \nabla\phi - \phi(1-\phi)\boldsymbol{n}] \tag{6}$$

where ϕ is level set variable whose value lies between 0 (pure CP) to 1 (pure DP). ϵ_{ls}, and γ are level set parameters which accounts for re-initialization and stabilization of level set function ϕ, and interface thickness. The properties of phases like density (ρ) and dynamic viscosity (μ) for the two-phase system are the function of level set variable (ϕ) defined as:

$$\alpha(\phi) = \alpha_c + (\alpha_d - \alpha_c)\phi \tag{7}$$

where α is the fluid property and the subscripts 'c' and 'd' refer to the continuous and dispersed phases, respectively. For accounting the surface tension forces between the two immiscible phases, the continuum surface force model [4] is employed as follows:

$$F_\sigma = \sigma\kappa\delta(\phi)\boldsymbol{n} \tag{8}$$

where σ is the surface tension coefficient (N/m), $\delta(\phi)$ is the Dirac delta function which is approximated as $\delta(\phi) = 6(|\nabla\phi|)|\phi(1-\phi)|$, $\kappa = R^{-1} = -(\nabla\cdot\boldsymbol{n})$ is the mean curvature, and $\boldsymbol{n}$ is unit normal.

2.3 Computational Approach

The computational model is built in a CFD solver, COMSOL multi-physics using finite element method. For each simulation, the time step (Δt) of 10^{-4} s is selected to find the iterative solution for two phase flow for following parameters:

1. Mesh attributes: Linear, non-uniform, unstructured, fine tetrahedral mesh, maximum mesh element size $\delta_{\max} = 30.6\ \mu$m with element count $N_{\mathrm{e}} = 137{,}278$ and degrees of freedom (DOF) = 158,122
2. Level set parameters: $\gamma = 1$ m/s, $\epsilon_{ls} = 11.85\ \mu$m.
3. Flow governing parameters: $\rho_r = 0.998$; $\theta = 120°$, 135°; $Q_r = 0.667$ and 1; $\mu_r = 3.5$; $\mathrm{Ca}_c < 10^{-4}$; $\sigma = 10$ mN/m.

3 Results and Discussion

The results elucidated in this study are taken after the first droplet formation. The results are presented in terms of the phase, pressure, velocity magnitude and recirculation zone contours.

3.1 Phase Profiles

The phase flow contours predicting the second droplet pinch-off and breakup time and its movement along the channel at two different contact angles ($\theta = 120°$ and 135°) and flow rate ratios under squeezing regime are presented in Fig. 2. The onset of droplet formation is marked by the evolution, followed by steady growth of the dispersed phase into the continuous phase. Because of this phenomenon competing forces, i.e., the shear as well as the pressure buildup takes place which is followed by droplet pinch-off. Since the study is performed under the squeezing regime ($Ca_c < 10^{-3}$), the shear stress effects exerted on the interface of the emerging dispersed phase are negligible, because of which the dispersed phase grows into the continuous phase until it completely blocks the main channel resulting into the pressure buildup at the upstream resulting into droplet formation. From the phase contours, as the contact angle is increased from $\theta = 120°$ to 135°, there is change in the curvature of the droplet at the rear end. For $\theta = 120°$, the curvature is more convex at the rear end at the pinch-off stage. As the contact angle is increased, the curvature is more on the concave side. This is because, at the lower contact angle, the interaction of the fluid and the surface is more, hence more volume of the dispersed phase is interacting with the channel wall resulting into convex rear end.

The effect of changing the flow rate of the dispersed phase on the droplet breakup, for both the contact angle is not much pronounced but the time required by the droplet to stabilize for $\theta = 120°$ is 6 folds more as the dispersed phase flow rate is decreased from 15 to 10 μl/min. But the same pattern is not followed when $\theta = 135°$. This may be attributed to the reason that, as the contact angle is decreased more dispersed phase is entering continuous phase resulting in more time to stabilize.

3.2 Droplet Length

The data for the droplet lengths at the pinch-off time and the stabilizing time is presented in Table 1. From the table, it can be predicted that at low value of the contact angle ($\theta = 120°$), the breakup time is comparatively less than that for $\theta = 135°$ because at low contact angle more surface and interface interaction occur leading to less breakup time and larger droplet size. Also, there is no effect of increasing the flow rate of dispersed phase on the length of the droplet when $\theta = 120°$ but on

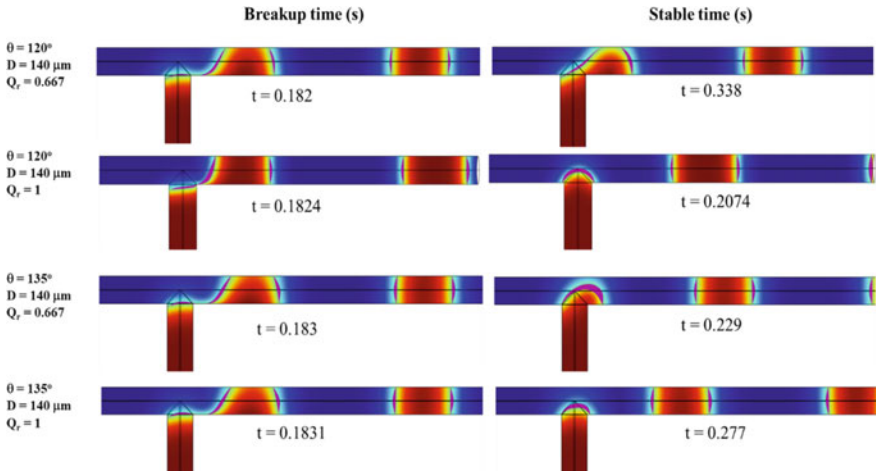

Fig. 2 Phase profiles for the breakup and stable droplet formation stages at various flow rate ratios for $\theta = 120°$

Table 1 Droplet length and breakup time

θ	Channel dia. (μm)	Flow rate ratio	Breakup time (s)	Breakup length (μm)	Stable time (s)	Stable droplet length (μm)
120°	140	0.667	0.182	302.7	0.338	321.5
120°	140	1	0.1824	302.1	0.2074	321.5
135°	140	0.667	0.183	324	0.229	314.3
135°	140	1	0.1831	304	0.227	324.1
120°	280	0.667	1.389	621.4	1.657	680.2
120°	280	1	1.392	615.9	1.602	687.4

increasing the contact angle, there is significant effect of the flow rate of the dispersed phase on the droplet size.

3.3 Instantaneous Pressure Profiles

This section elucidates the instantaneous pressure profiles in the dispersed, continuous and the droplet phases. The probe points for measuring the pressure in dispersed, continuous and droplet phases are taken at 300 μm upstream and downstream of the junction as shown in Fig. 1. The point pressures for all the phases, i.e., p_{dp}, p_{cp}, p_{drop} are converted into non-dimensional quantities using viscous shear term as:

$$P = p/\left(\frac{\mu_c u_c}{D_c}\right) \tag{10}$$

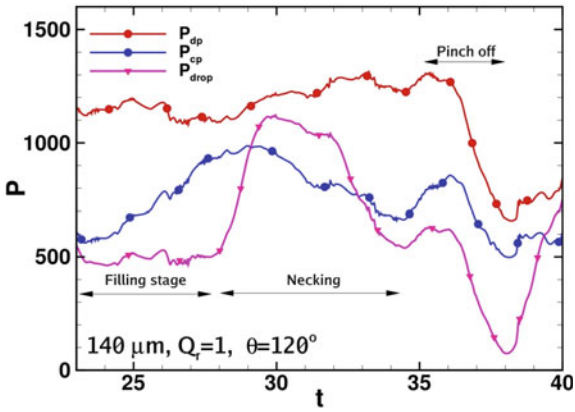

Fig. 3 Point pressure profiles in dispersed, continuous and droplet phases during droplet formation at $\theta = 120°$ and $Q_r = 1$ for $D = 140\ \mu m$

The droplet formation is marked by the entry of the dispersed phase into the continuous phase (filling stage) until it expands to the entire channel cross section, followed by the elongation of the dispersed phase into downstream (necking) and hence the pinch-off. The point pressure profiles for all the phases are elucidated in Fig. 3.

As the dispersed phase tip starts entering the main channel, there is resistance in the flow of the continuous phase resulting into the pressure buildup in the upstream section of the channel. This pressure buildup continuous till the channel is completely blocked by the dispersed phase. Till this point, the dispersed phase elongated thread reaches its critical thickness and pinches off resulting in the sudden drop in pressure in the dispersed phase.

From the Fig. 4, it can be seen that, during the entire process of droplet generation, there is no substantial change in the dispersed phase pressure values except for the point when there is sudden drop in the pressure values because of the pinch-off. The aforementioned trend is shown for both the flow rate ratios and the contact angle values. This result is reconcilable with the assumptions used by Garstecki et al. [7].

From Fig. 5, it can be seen that there is negligible effect of changing the dispersed phase flow rate on the point pressure profile, but the effect of increasing the contact angle is profound. As discussed before, as the contact angle is increased, there is change in the rear end curvature of the droplet from convex to more concave. Thus, at the rear end, there exists less pressure at lower contact angle ($\theta = 120°$).

3.4 Velocity Profiles and Recirculation Zones

In the squeezing regime, during the droplet formation, the impact of pressure build up is more substantial as compared to the shear stress values. The droplets formed are in shape of plugs that inhabit the entire cross section of the main channel.

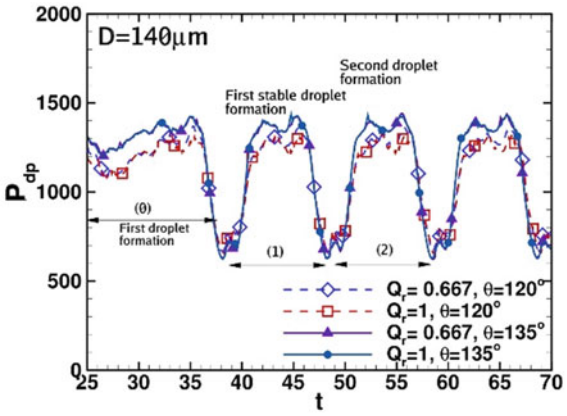

Fig. 4 Point pressure profiles in dispersed phase at various contact angles (θ) and flow rate ratios Q_r for D = 140 μm

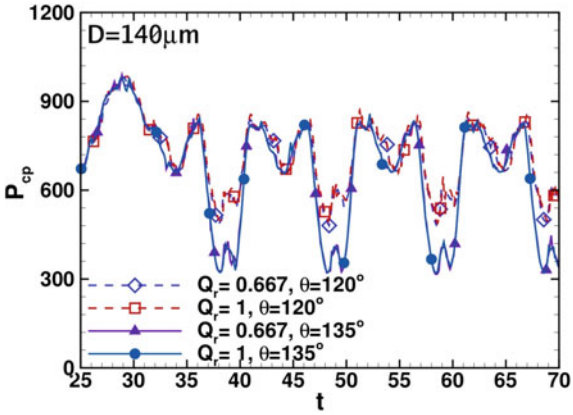

Fig. 5 Point pressure profiles in continuous phase at both contact angles (θ) and flow rate ratios Q_r for D = 140 μm

In the first two contours in Figs. 7, 8 and 10, the droplet phase slowly emerges into the main channel, forming a thread which grows gradually as the continuous phase proceeds downstream. This causes implosion for the continuous phase resulting into the formation of recirculation zones. From Fig. 9, it can be predicted that the fluctuation in the velocity magnitude is more pronounced when the continuous phase flow rate is higher keeping the channel dimension and contact angle same. This is because at high Q_c, the flow of continuous phase around the dispersed phase will be more pronounced leading to higher intensity recirculation zones as shown in first two contours in Figs. 7 and 8. The onset of the necking stage is marked by the departure of the thread tail from the upstream side as shown in Fig. 6c marked by the first crest, i.e., point (i) in velocity magnitude (Fig. 9). The necking proceeds until the droplet detachment starts marked by the stage when the neck width reaches its critical value. Right after the droplet detachment, a large recirculation zone evolve, caused by the flinching of the dispersed phase thread and the surface tension forcing the droplet to form the stable curvature. The large recirculation corresponds to the sudden velocity

spike as shown with point (ii) in Fig. 9. Also, on comparing Figs. 7 and 10, it can be seen that the more recirculation zones are formed when the channel dimensions are increased two fold keeping the flow rate constant. This can be because of the increased Reynolds number.

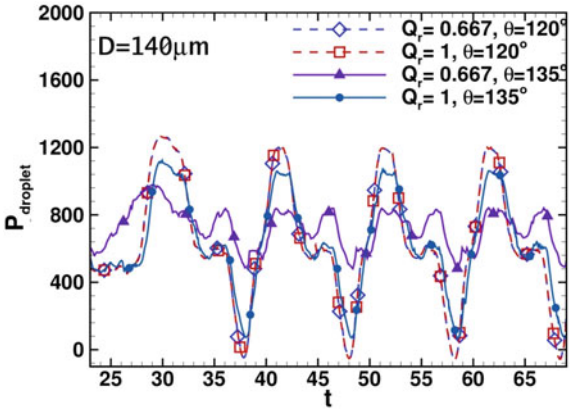

Fig. 6 Point pressure profiles in droplet phase at both contact angles (θ) and flow rate ratios Q_r for $D = 140$ μm

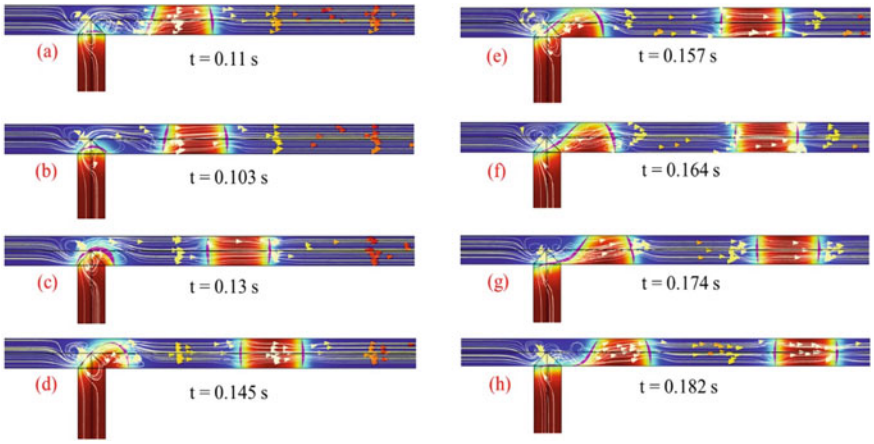

Fig. 7 Recirculation zones formation during dispersed phase evolution and droplet pinch-off for $D = 140$ μm at $Q_r = 0.667$

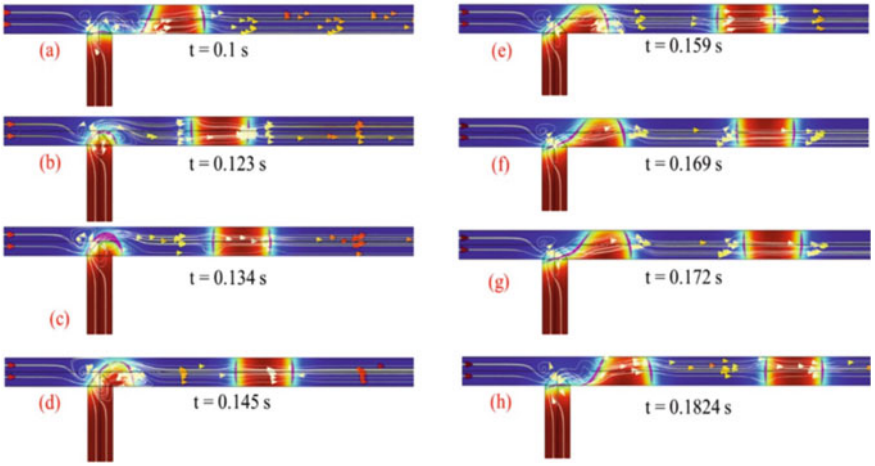

Fig. 8 Recirculation zones formation during dispersed phase evolution and droplet pinch-off for $D = 140$ μm at $Q_r = 1$

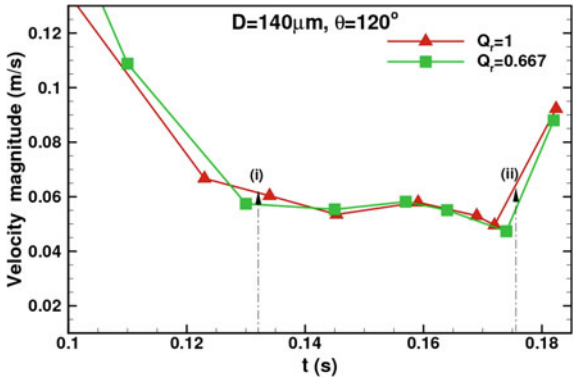

Fig. 9 Comparison of velocity magnitude over time for $Q_d = 15$ μl/min and 10 μl/min with fixed $Q_c = 15$ μl/min

4 Conclusions

In the present study, a cylindrical microfluidic cross-flow T-junction geometry is studied for two flow rate ratios and contact angles. It can be elucidated that, variation in the contact angle does not have very substantial effect on the droplet shape, size but there is significant change in the time taken by the droplets to stabilize and bring in equilibrium curvature. Also, it can be predicted that because of the change in the droplet curvature owing to lower contact angle, the magnitude of the pressure drop in the continuous phase is substantially low.

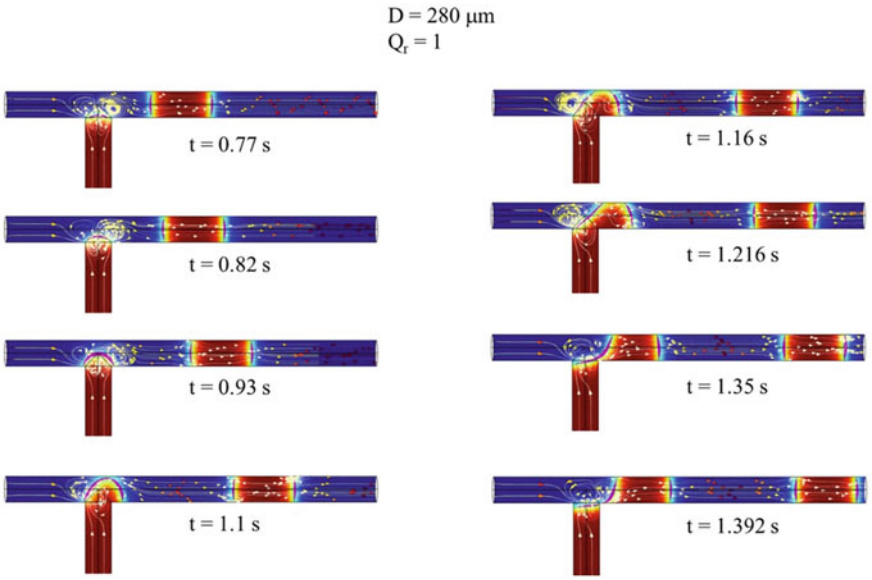

Fig. 10 Recirculation zones formation during dispersed phase evolution and droplet pinch-off for $D = 280$ μm at $Q_r = 1$

References

1. Jena SK, Bahga SS, Kondaraju S (2021) Prediction of droplet sizes in a T-junction micros channel: Effect of dispersed phase inertial forces. Phys Fluids 33:032120
2. Lei L, Zhao Y, Chen W, Li H, Wang X, Zhang J (2021) Experimental studies of droplet formation process and length for liquid–liquid two-phase flows in a microchannel. Energies 14:1341
3. Garstecki P, Fuerstman MJ, Stone HA, Whitesides GM (2006) Formation of droplets and bubbles in a microfluidic T-junction scaling and mechanism of break-up. Lab on Chip 6:437–446
4. Brackbill JU, Kothe DB, Zemach C (1992) A continuum method for modeling surface tension. J Comput Phys 100:335–354
5. Anna SL, Bontoux N, Stone HA (2003) Formation of dispersions using "flow focusing" in microchannels. Appl Phys Lett 82:364–366
6. Whitesides GM (2006) The origins and the future of microfluidics. Nature 442:368–373
7. Thorsen T, Roberts RW, Arnold FH, Quake SR (2001) Dynamic pattern formation in a vesicle-generating microfluidic device. Phys Rev Lett 86:4163
8. Cramer C, Fischer P, Windhab EJ (2004) Drop formation in a co-flowing ambient fluid. Chem Eng Sci 59:3045–3058
9. Christopher GF, Noharuddin NN, Taylor JA, Anna SL (2008) Experimental observations of the squeezing-to-dripping transition in T-shaped microfluidic junctions. Phys Rev E 78:036317
10. Li X, He L, He Y, Gu H, Liu M (2019) Numerical study of droplet formation in the ordinary and modified T-junctions. Phys Fluids 31:082101
11. Venkateshwarlu A, Bharti RP (2022) Interface evolution and pinch-off mechanism of droplet in two-phase liquid flow through T-junction microfluidic system. Colloids Surf A Physicochem Eng Asp 642:128536
12. Umbanhowar P, Prasad V, Weitz DA (2000) Monodisperse emulsion generation via drop break off in a coflowing stream. Langmuir 16:347–351

13. Kovalev V, Yagodnitsyna AA, Bilsky AV (2018) Flow hydrodynamics of immiscible liquids with low viscosity ratio in a rectangular microchannel with T- junction. Chem Eng J 352:120–132
14. Bashir S, Rees JM, Zimmerman WB (2014) Investigation of pressure profile evolution during confined microdroplet formation using a two-phase level set method. Int J Multiph Flow 60:40–49
15. Kalantarifard, Alizadeh-Haghighi E, Saateh A, Elbuken C (2021) Theoretical and experimental limits of monodisperse droplet generation. Chem Eng Sci 229:116093
16. De Menech M, Garstecki P, Jousse F, Stone HA (2008) Transition from squeezing to dripping in a microfluidic T-shaped junction. J Fluid Mech 595:141–161
17. Wu Y, Fu T, Zhu C, Ma Y, Li HZ (2014) Bubble coalescence at a microfluidic T-junction convergence: from colliding to squeezing. Microfluid. Nanofluidics 16:275–286